Electronic Supplementary Material (ESI) for Inorganic Chemistry Frontiers.

Supporting information

Manipulating photon absorption and trap energy supply for multimode dynamic anti-counterfeiting

*Zhihao Zhang,[a,b] Huimin Li,[*a] Ran Pang,[a] Da Li,[a] Lihong Jiang,[a] Su Zhang[*a,b] and Hongjie Zhang[a]*

[*] Corresponding authors.

E-mail addresses: huiminlihector@gmail.com (Huimin Li); zhangsu@ciac.ac.cn (Su Zhang).

[a] State key Laboratory of Rare Earth Resource Utilization, Changchun Institute of Applied Chemistry, Chinese Academy of Sciences, Changchun 130022, P. R. China

[b] School of Applied Chemistry and Engineering, University of Science and Technology of China, Hefei 230026, China

Experimental Section

Materials and Sample Synthesis:

The $Y_{2-x}CaSnGa_4O_{12}:xPr^{3+}$ was synthesized by high-temperature solid-state reaction method. The raw materials are Y_2O_3 (99.99%, Aladdin), $CaCO_3$ (99.99%, Aladdin), SnO_2 (99.5%, Aladdin), Ga_2O_3 (99.999%, Suzhou Kangpeng), and Pr_6O_{11} (99.99%,). They were stoichiometrically mixed and grinded in an agate mortar until homogeneous. Then the mixture was placed in an alumina crucible and sintered in a muffle furnace at 1450 ℃ for 6 hours. After cooling to room temperature, grind it for 5 minutes with an agate mortar for subsequent testing.

Characterizations:

X-ray diffraction (XRD) patterns were obtained by a United Kingdom - Malvenpa - Naco New generation X'Pert³ diffractometer equipped with Cu Kα radiation at 40 kV and 40 mA (λ = 0.15405 nm). Concentration-dependent PL spectra were measured by a F7000 fluorescence spectrophotometer. Temperature-independent spectra were measured by a FLS 920 fluorescence spectrophotometer (Edinburgh Instruments) equipped with a 450 W xenon lamp and a temperature control device. Thermoluminescence (TL) curves were recorded by a CCD detector equipped with a heating device. Afterglow spectra were recorded at different temperatures by adjusting the temperature settings of the heating device. The relevant parameters of L*a*b* (1976) were measured by CS-821N high stability desktop spectrophotometer with D65 light source (Hangzhou Color Spectrum Technology Co. Ltd) and ensure that the test surfaces of the samples are uniform in size and smooth (specific quality in a quartz container or be pressed into a specific size piece). UV-vis diffuse reflectance spectra (DRS) were measured on a UV–vis spectrophotometer (Agilent Cary 7000) using $BaSO_4$ as the reference. In the process of taking photos, long wave pass 495nm filter and 350nm filter are used to block the mobile phone camera to shield the excited light. The ultraviolet radiation meter (LS125, Shenzhen Linshang Technology Co. Ltd) equipped with two probes (UVCLED-X0 for 230-340 nm and UVALED-X3 for 330-

420 nm) was used to measure the irradiation power of light sources with different wavelengths. The spectral response characteristic curve is a key parameter for the performance of an ultraviolet radiation meter. It refers to the ratio between the measured intensity to the actual incident intensity when the detection window is illuminated by light of different wavelengths. Its value close to 100% proves the high accuracy of the measured irradiation intensity. For the visible light region, there is no irradiance meter available, so we measure the luminous flux to ensure that the irradiation power of light sources of different wavelengths is the same. The conversion formula is as follows:

$$Luminous\ flux = K_m \times V(\lambda) \times Radiant\ Flux$$

$$Radiant\ Flux = Irradiation\ density\ \times Irradiated\ area$$

K_m is the maximum value of spectral light visual efficiency, which is equal to 683 lm/W. *V(λ)* is the standard spectral efficiency function for photopic vision specified by the International Commission on Illumination (CIE), with a maximum value of 1. The unit of Radiant Flux is W, which can be decomposed into the product of Irradiation density (W/cm^2) and Irradiated area (cm^2). The EPR measurement were carried by the Bruker EMXnano electron paramagnetic energy spectrometer. XPS spectra were obtained by an Agilent 5110(OES) X-ray photoelectron spectrometer before and after coloration.

Figures and Tables

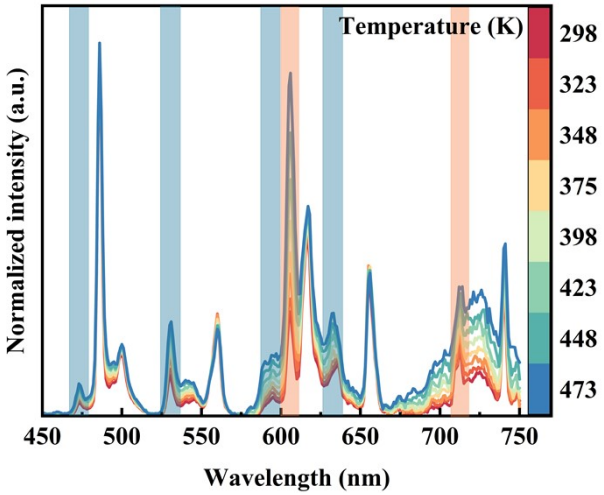

Figure S1. Normalized temperature-dependent PL spectra of YCSG:0.001Pr^{3+}.

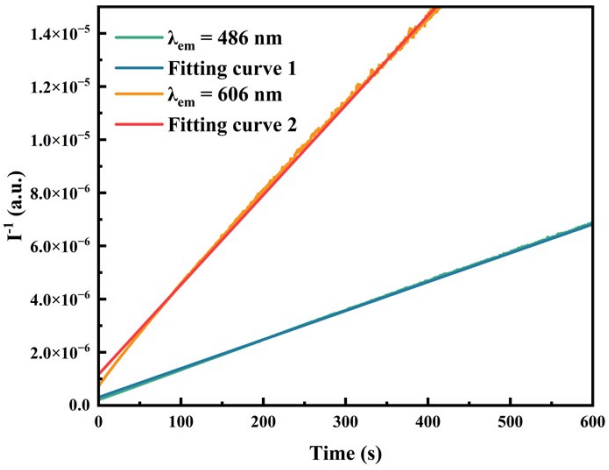

Figure S2. The linear fitting results of afterglow decay curve ($I^{-1} \propto t$).

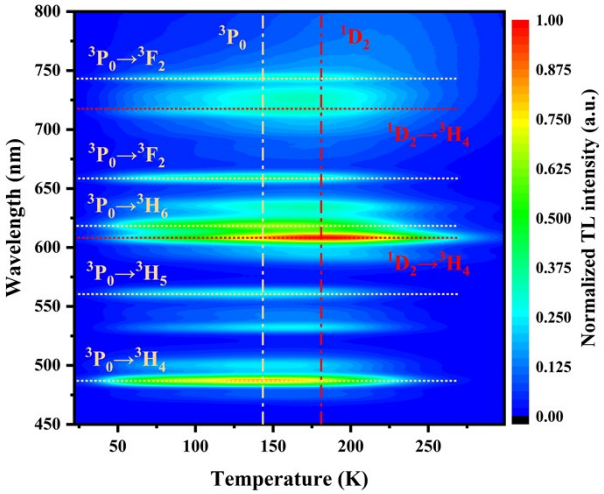

Figure S3 2D-TL spectra of YCSG:0.001Pr^{3+}.

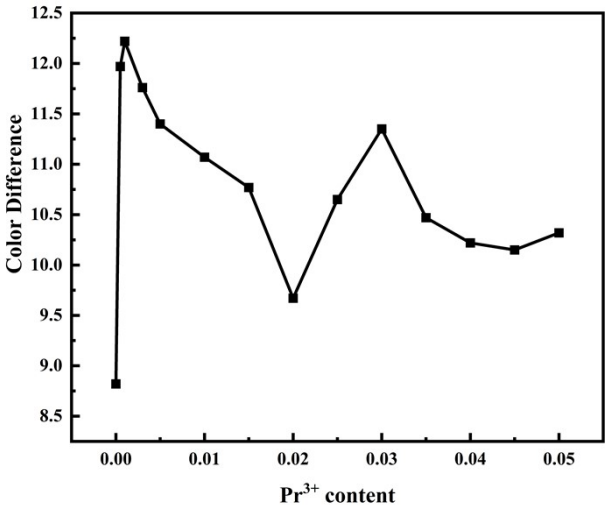

Figure S4. The color difference of YCSG:xPr^{3+} before and after irradiation.

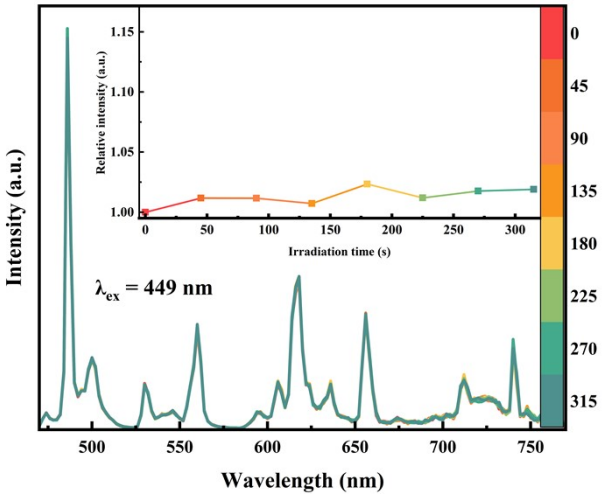

Figure S5. Irradiation time-dependent PL spectra of YCSG:0.001Pr^{3+} under the excitation of 449 nm light. The inset shows the relative intensity of integrated PL spectra with 449 nm light irradiation time.

Table S1. colorimetric parameters L*, a* and b* of YCSG:xPr^{3+}.

x	indoor light			254nm irradiated for 5min			ΔE
	L*	a*	b*	L*	a*	b*	
0	97.37	0	0.46	89.46	0.53	4.35	8.82
0.0005	97.04	-0.36	1.31	88.46	2.02	9.3	11.97
0.001	97.17	-0.36	1.48	88.29	2.15	9.48	12.22
0.003	98.22	-0.66	2.09	90.38	2.37	10.31	11.76
0.005	98.06	-0.84	2.28	90.67	2.4	10.33	11.4
0.01	98.1	-1.31	3.32	90.76	2.25	10.8	11.07
0.015	97.83	-1.59	3.91	90.75	2.16	11.11	10.77
0.02	97.38	-2.1	4.86	90.83	1.77	10.83	9.67
0.025	97.1	-2.56	5.65	89.62	1.93	11.76	10.65
0.03	96.75	-3.03	6.42	88.89	1.94	12.92	11.35
0.035	97.1	-2.99	6.5	89.71	1.56	12.36	10.47
0.04	97.1	-3.25	6.9	89.84	1.28	12.47	10.22
0.045	96.79	-3.43	7.21	89.62	1.36	12.56	10.15
0.05	96.79	-3.63	7.44	89.59	1.18	13.07	10.32

*The power density of the light source with wavelength of 254 nm is ~ 2 mW/cm^2.

Part 1. Choice of Colorimetric Parameter.

Changes in the color of opaque materials are usually caused by changes in the composition and number of photons absorbed or reflected. However, we know that the light that can be resolved by the naked eye is distributed over a wide spectral range, and the human eye is sensitive to different wavelengths of light. This makes the current method of measuring color difference based on the maximum difference of change in reflection or absorption spectrum (ΔAbs) inaccurate. A similar situation is to compare the brightness of a material with line-type emission and a material with broad band emission. Obviously, the emission intensity at a certain wavelength cannot be used as the reference. It may be more appropriate to use the magnitude of the integrated intensity as a standard. However, even if the integral intensity is the same, if the emission peak position is different, the difference in sensitivity of the human eye to different wavelengths of light will make people feel that the brightness of the two is different. In short, color is a broad concept for the spectrum, the intensity change in certain wavelength is too narrow to describe it.

Taking YCSG:Cr^{3+} and YCSG:Pr^{3+} that show different color as examples, the changes of colorimetric parameters were shown in Figure S6. Obviously, the color centers of them exhibit different photon absorption tendencies: For the colored YCSG:Pr^{3+}, it mainly absorbs blue-violet light located near 400 nm, while YCSG:Cr^{3+} is blue-violet light and green light. The corresponding colors vary from light green to brown (YCSG:Pr^{3+}) and grayish green to pink (YCSG:Cr^{3+}). YCSG:Cr^{3+} and YCSG:Pr^{3+} show significant difference for ΔAbs, while smaller difference for color difference in L*a*b* color space. As can be seen from the color changes shown in the inset, the color difference before and after the color change for them is obviously not very different. This can show that using the maximum difference of ΔAbs at a specific wavelength to assess the color difference is not so accurate.

Certainly, we do not think that previous work using the maximum difference of ΔAbs at a specific wavelength to assess the color difference is unscientific. At present, most colored photochromic materials are brown-gray, which ensure the similar photon absorption within the spectral range. And L*a*b* color space is usually used when

describing complex color variations.[1-3] We point out the shortcomings of this method in this work only to remind this often overlooked point and provide an alternative.

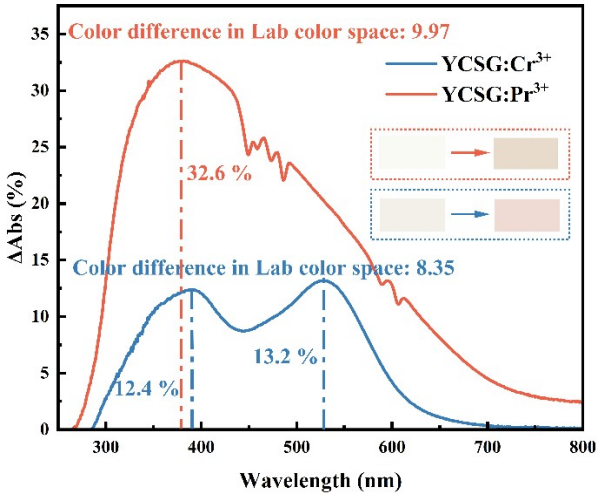

Figure S6. Parameter changes of YCSG:Cr^{3+} and YCSG:Pr^{3+} before and after coloration.

Part 2. Calculation of Optical Band Gap Energy

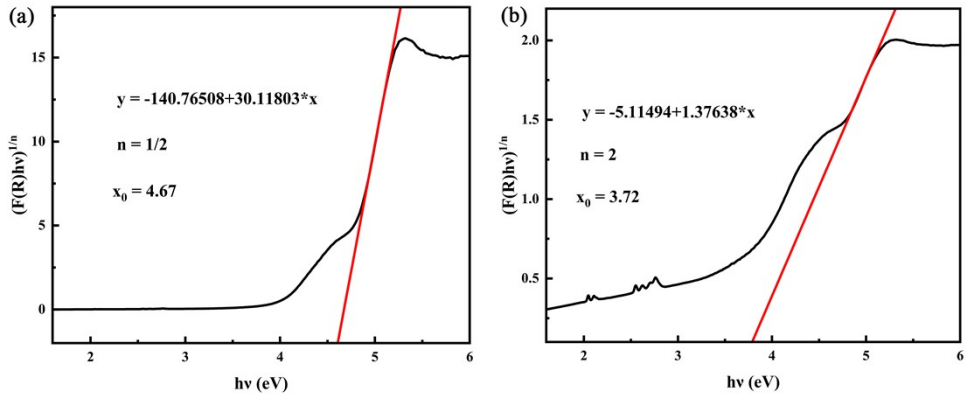

Figure S7. Tauc plot for YCSG:0.01Pr^{3+} when n_0 = 1/2 (a) and 2 (b).

The optical energy band gap E_g can be roughly calculated by Kubelka-Munk function based on the DRS:

$$(F(R)h\nu)^{1/n_0} = \frac{K}{S} = \frac{(1-R)^2}{2R} = B(h\nu - E_g) \quad (1)$$

K is the absorption coefficient, S is the reflection coefficient, R is the reflectivity (percentage form), where h is Planck's constant, ν is the frequency of light, E_g is a physical quantity related to the material, that is, the band gap energy value. n_0 for indirect bandgap semiconductors it is 2, for direct bandgap semiconductors it is 1/2. Taking $(F(R)h\nu)^{1/n_0}$ as the ordinate, hν as the abscissa, to obtain a linear equation whose intercept on the x-axis is the magnitude of the bandgap energy. As shown in Figure S15, the optical energy gap can be estimated as 4.67 and 3.72 for the value of n_0 is 1/2 and 2 (Figure S7). However, as shown in Figure 6c of revised manuscript, the light with wavelength of 333 nm (3.72 eV) can hardly charge the traps, then the optical band gap is estimated as 4.67 eV.

Part 3. Origination of Color Centers and Traps

From a functional point of view, the color center is a unit that can absorb photons. After the formation of the color center, it can absorb the photons that are illuminated on the material, causing the color of the material to change. In essence, it is a unit formed after the carrier is trapped in a variety of defects, which requires external photon irradiation to help the carrier desorption, usually from sources including: lattice defects[4-6] or the valence state change of ions.[7, 8] The Electron Paramagnetic Resonance (EPR) and X-ray photoelectron spectroscopy (XPS) were employed to explore changes of valence state and oxygen vacancies before and after coloration.

EPR spectra of the samples before and after irradiation are shown in Figure S8a and Figure S8b, the signal of ionized oxygen vacancy (g = 1.995) is obviously observed,[7] indicating that the oxygen vacancies in sample capture free electrons after 254 nm light irradiation.[9] This phenomenon occurs in samples with and without doping, indicating the presence of PC phenomenon highly related to oxygen vacancy.

The high-resolution XPS spectra for O 1s of YCSG and YCSG:0.01Pr^{3+} are shown in Figure S8d and Figure S8e. Both of them can be well fitted into three peaks, indicating the three kinds of chemical environments for oxygen atoms. The three peaks located at ~530.4, ~531.6 and ~532.9 eV can be attributed to lattice oxygen, oxygen vacancy and the adsorbed O_2 molecules (interstitial oxygen), respectively.[10, 11] As the detailed results of XPS peak fitting listed in Table S2, the area percentage of oxygen vacancy (~531.6 eV) decrease from 49.96 % to 28.67 % after being irradiated by UV light in YCSG, from 49.70 % to 44.39 % after being irradiated by UV light in YCSG:0.01Pr^{3+}. The small reduction of area proportion corresponding to oxygen vacancy in YCSG:0.01Pr^{3+} may be related to the valence state change of Pr^{3+}. The high-resolution XPS spectra for Pr 3d are shown in Figure S9. The area percentage of Pr^{3+} increase from 83.72 % to 84.25 % after the irradiation, indicating a slightly reduction in Pr^{4+} content. Therefore, the complex traps and compositional changes after the introduction of Pr^{3+} lead to the decline of the oxygen vacancy area proportion.

According to the above results, it can be deduced that the mechanism of PC

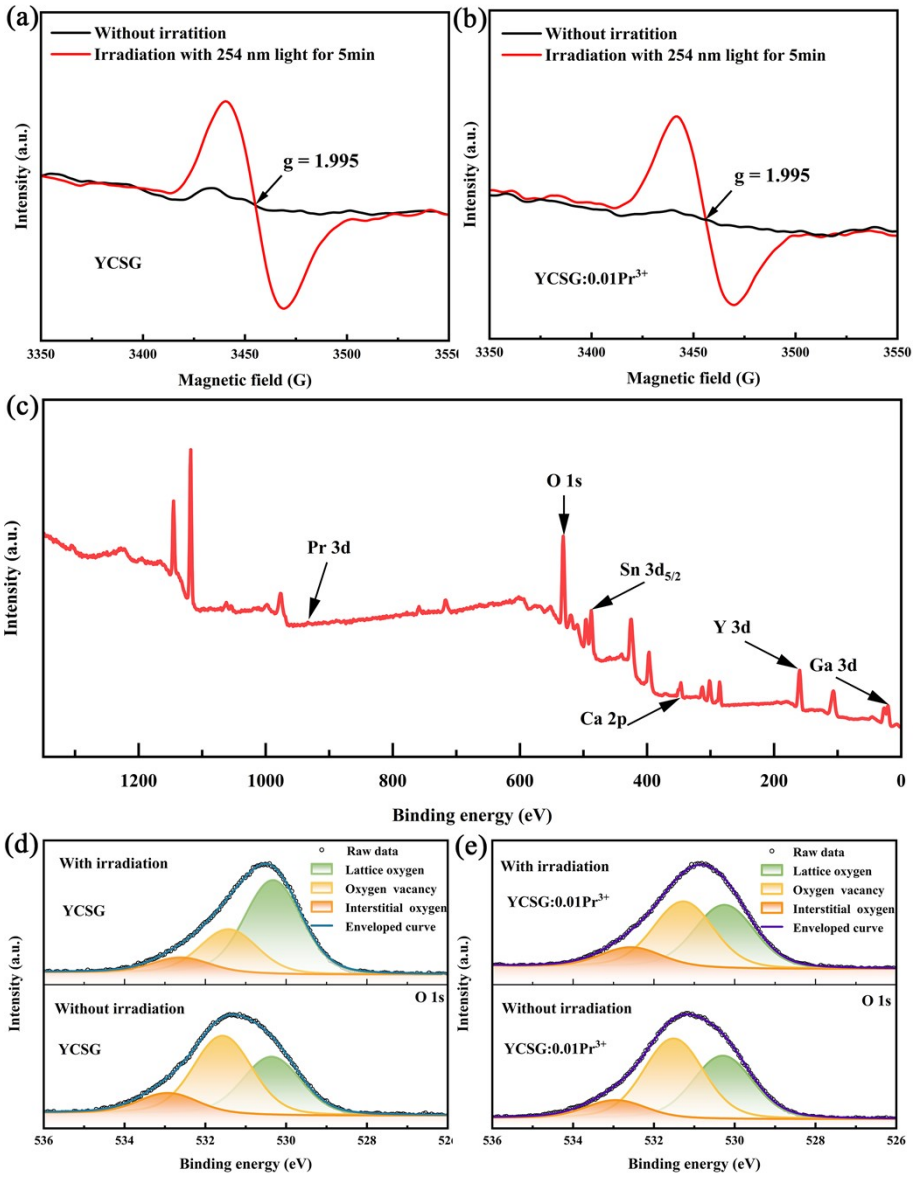

Figure S8. EPR spectra of (a) YCSG and (b) YCSG:0.01Pr^{3+} with or without irritation by UV light; (c) XPS survey spectra of YCSG:0.01Pr^{3+}. (d) High-resolution XPS spectra at binding energy for O 1s of (d) YCGS and (e) YCSG:0.01Pr^{3+} with or without irritation by UV light.

phenomenon is as follows: Under the excitation of high-energy photons, some ions and defects in the crystal cell are photoionized, leaving free holes at the valence band (VB) and free electrons at the conduction band (CB). These free carriers are then trapped by traps with opposite charge, such as the positively charged oxygen vacancies and negatively charged Ga^{3+} vacancies.[12] In addition, Pr^{4+}/Pr^{3+} may also act as carrier

Table S2. The peak fitting results of high-resolution O1s XPS spectra in YCSG and YCSG:0.01Pr^{3+}.

	Without irritation			With irritation		
	Pos. (eV)	FWHM (eV)	Area%	Pos. (eV)	FWHM (eV)	Area%
YCSG	530.36	1.70	37.29	530.32	1.66	61.52
	531.57	1.70	49.96	531.42	1.66	28.67
	532.92	1.70	12.75	532.61	1.66	9.80
YCSG: 0.01Pr^{3+}	530.38	1.74	39.24	530.25	1.75	42.69
	531.60	1.74	49.70	531.27	1.75	44.39
	533.03	1.74	11.06	532.57	1.75	12.92

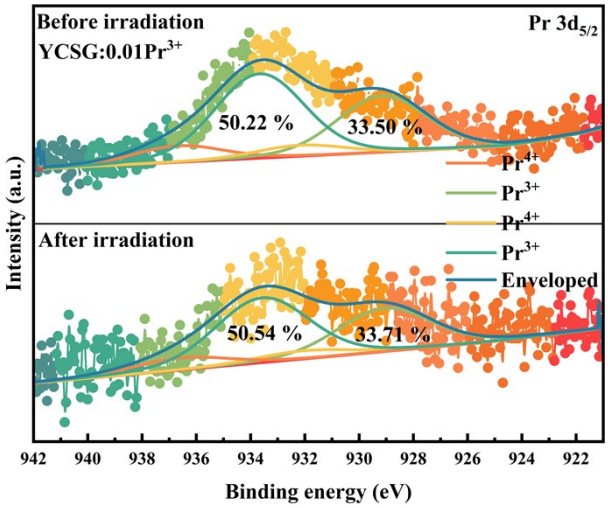

Figure S9. High resolution XPS spectra of Pr 3d5/2 and the fitting curves of YCSG:0.01Pr^{3+}.

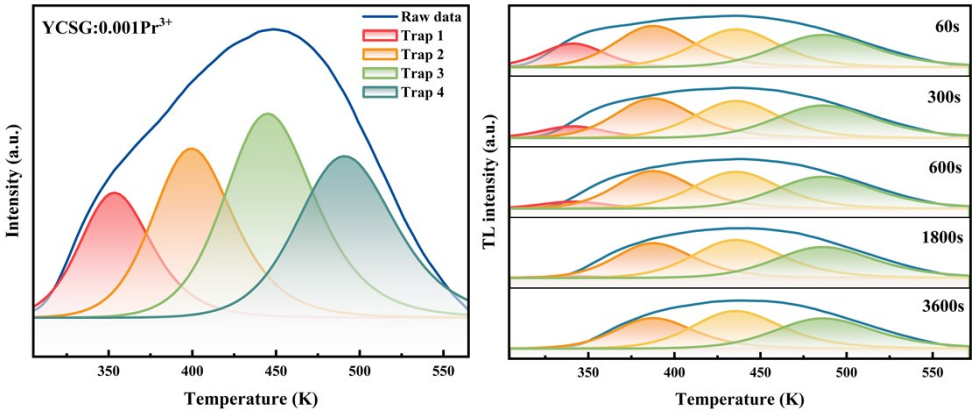

Figure S10. (a) TL curve and kinetic fitting results of YCSG:0.001Pr^{3+}. (b) Kinetic fitting curves of TL curves of YCSG:0.001Pr^{3+} after different delay time.

traps due to the mixed valence state of Pr. These traps are capable of absorbing photons from outside to form color centers, which has been widely adopted in previous reports.[13, 14] Therefore, the charging and discharging process of the traps plays a vital role in the coloration and bleaching processes.

Trap is a general term for a defect capable of trapping charge carriers, which can provide energy to the luminescence centers through energy band or quantum tunneling channel under the action of thermal stimulation and therefore produce afterglow without excitation light. TL is a well-established means to characterize the trap state.[15] The TL curves of YCSG:0.001Pr^{3+} after irradiation by 254 nm light for 5 min is shown in Figure 8a. The broad trap distribution suggests that it consists of multiple traps, and this phenomenon still exists after a period of decay (Figure S10b). GCD analysis is a common method to analyze the TL curve, which is widely used in the fields of dosimetry, environmental monitoring and optical information storage.[16-18] The TL curve was fitted by a general-order TL kinetic equation built in a homemade software package, which can be expressed as Equation. (3):[19]

$$I(T) = n_0 S exp\left(-\frac{E}{kT}\right)\left[(b-1)\left(\frac{S}{\beta}\right)\int_{T_0}^{T} exp\left(-\frac{E}{kT}\right)dT + 1\right] \qquad (3)$$

I(T) is the TL peak intensity, E is the activation energy (equal to the trap depth), S is the frequency factor. n_0 is the initial concentration of trapped charges in cm^{-1}. The k is the Boltzmann constant (8.617×10-5 eV/K), T is the absolute temperature (K). β is the heating rate (3K/s). The b is the kinetic order, which can be predicted from the peak shape symmetry parameter (μ).[20] The fitting results are plotted in Figure 4a, showing four distinct peaks (named as trap1-4 from shallow to deep). The trap depths of these four peaks are 0.7,0.793, 0.885 and 0.976 respectively. And their trap densities are 1.52×10^7, 2.33×10^7, 3.12×10^7 and 2.66×10^7, respectively. These traps may be associated with the loss of ions[21], unequal substitution[22] and valence transition[23] during sintering. However, there is currently no proper way to distinguish between these traps. Moreover, the characterization of trap usually needs to be carried out after irradiation of ultraviolet light which can cause photochromism, so it is difficult to distinguish

whether the change of corresponding parameters is caused by trap or color center.

Reference

1. H. C. Byron, C. Swain, P. Paturi, P. Colinet, R. Rullan, V. Halava, T. Le Bahers and M. Lastusaari, Highly tuneable photochromic sodalites for dosimetry, security marking and imaging, *Advanced Functional Materials*, 2023, **33**, 2303398.
2. M. Back, J. Xu, J. Ueda, A. Benedetti and S. Tanabe, Thermochromic Narrow Band Gap Phosphors for Multimodal Optical Thermometry: The Case of Y^{3+}-Stabilized β-Bi_2O_3:Nd^{3+}, *Chemistry of Materials*, 2022, **34**, 8198-8206.
3. T. Chen, B. Xu, M. Zhu, J. Zhang, W. Sun and J. Han, Advanced functional photochromic wearables with fast photo-responsivity, long color-retention, and multi-environmental stability, *Chemical Engineering Journal*, 2024, **490**, 151804.
4. A. A. Haider, Y. Cun, X. Bai, Z. Xu, Y. Zi, J. Qiu, Z. Song, A. Huang and Z. Yang, Anti-counterfeiting applications by photochromism induced modulation of reversible upconversion luminescence in TiO_2:Yb^{3+},Er^{3+} ceramic, *Journal of Materials Chemistry C*, 2022, **10**, 6243-6251.
5. L. Yuan, Y. Jin, D. Zhu, Z. Mou, G. Xie and Y. Hu, Ni^{2+}-doped yttrium aluminum gallium garnet phosphors: Bandgap engineering for broad-band wavelength-tunable shortwave-infrared long-persistent luminescence and photochromism, *ACS Sustainable Chemistry & Engineering*, 2020, **8**, 6543-6550.
6. Y. Ren, Z. Yang, Y. Wang, M. Li, J. Qiu, Z. Song, J. Yu, A. Ullah and I. Khan, Reversible multiplexing for optical information recording, erasing, and reading-out in photochromic $BaMgSiO_4$:Bi^{3+} luminescence ceramics, *Science China Materials*, 2020, **63**, 582-592.
7. V. Laguta, M. Buryi, P. Arhipov, O. Sidletskiy, O. Laguta, M. G. Brik and M. Nikl, Oxygen-vacancy donor-electron center in Y3Al5O12 garnet crystals: Electron paramagnetic resonance and dielectric spectroscopy study, *Physical Review B*, 2020, **101**.
8. Z. Hu, X. Huang, ZhengwenYang, J. Qiu, Z. Song, J. Zhang and G. Dong, Reversible 3D optical data storage and information encryption in photo-modulated transparent glass medium, *Light: Science & Applications*, 2021, **10**, 140-149.
9. Q. Du, J. Ueda, R. Zheng and S. Tanabe, Photochromism and long persistent luminescence in Pr^{3+}-doped garnet transparent ceramic via uv or blue light up-conversion charging, *Advanced Optical Materials*, 2023, **11**, 2202612.
10. X. Xue, R. Chen, H. Chen, Y. Hu, Q. Ding, Z. Liu, L. Ma, G. Zhu, W. Zhang, Q. Yu, J. Liu, J. Ma and Z. Jin, Oxygen Vacancy Engineering Promoted Photocatalytic Ammonia Synthesis on Ultrathin Two-Dimensional Bismuth Oxybromide Nanosheets, *Nano Letters*, 2018, **18**, 7372-7377.
11. S. Gao, Z. Sun, W. Liu, X. Jiao, X. Zu, Q. Hu, Y. Sun, T. Yao, W. Zhang, S. Wei and Y. Xie, Atomic layer confined vacancies for atomic-level insights into carbon dioxide electroreduction, *Nature Communications*, 2017, **8**, 14503.
12. H. Li, R. Pang, Y. Luo, H. Wu, S. Zhang, L. Jiang, D. Li, C. Li and H. Zhang,

Structural Micromodulation on Bi3+-Doped Ba2Ga2GeO7 Phosphor with Considerable Tunability of the Defect-Oriented Optical Properties, *ACS Applied Electronic Materials*, 2019, **1**, 229-237.
13. Y. Ma, S. Yang, C. Zhao, C. Lin, J. Lin, X. Wu, M. Gao, T. Lin and C. Fang, Photochromic and Electric Field-Regulating Luminescence in High-Transparent (K,Na)NbO(3)-Based Ferroelectric Ceramics with Two-Phase Coexistence, *ACS Applied Materials & Interfaces*, 2022, **14**, 35940-35948.
14. Y. Zhu, H. Sun, Q. Jia, L. Guan, D. Peng, Q. Zhang and X. Hao, Site-selective occupancy of Eu^{2+} toward high luminescence switching contrast in $BaMgSiO_4$-based photochromic materials, *Advanced Optical Materials*, 2021, **9**, 2001626.
15. J. Du, O. Q. De Clercq and D. Poelman, Temperature dependent persistent luminescence: Evaluating the optimum working temperature, *Scientific Reports*, 2019, **9**, 10517.
16. M. Wazir-Ud-Din, S. Ur-Rehman, M. M. Mahmood, K. Ahmad, S. Hayat, M. T. Siddique, M. B. Kakakhel and S. M. Mirza, Computerized glow curve deconvolution (CGCD): A comparison using asymptotic vs rational approximation in thermoluminescence kinetic models, *Applied Radiation and Isotopes*, 2022, **179**, 110014.
17. E. G. Yukihara, A. J. J. Bos, P. Bilski and S. W. S. McKeever, The quest for new thermoluminescence and optically stimulated luminescence materials: Needs, strategies and pitfalls, *Radiation Measurements*, 2022, **158**.
18. L. Yuan, Y. Jin, Y. Su, H. Wu, Y. Hu and S. Yang, Optically Stimulated Luminescence Phosphors: Principles, Applications, and Prospects, *Laser & Photonics Reviews*, 2020, **14**.
19. T. Aitasalo, J. Holsa, H. Jungner, M. Lastusaari and J. Niittykoski, Thermoluminescence study of persistent luminescence materials Eu^{2+}-and R^{3+}-doped-calcium-aluminates, $CaAl_2O_4$:Eu^{2+},R^{3+}, *The Journal of Physical Chemistry B*, 2006, **110**, 4589-4598.
20. Y. Alajlani and N. Can, Thermoluminescence glow curve analysis and kinetic parameters of Dy-doped BaSi2O5 phosphor, *Journal of Rare Earths*, 2022, **40**, 234-242.
21. R. Hu, Y. Zhang, Y. Zhao, X. Wang, G. Li and C. Wang, UV–Vis-NIR broadband-photostimulated luminescence of LiTaO3:Bi3+ long-persistent phosphor and the optical storage properties, *Chemical Engineering Journal*, 2020, **392**, 124807.
22. Y. Zhuang, Y. Lv, L. Wang, W. Chen, T. L. Zhou, T. Takeda, N. Hirosaki and R. J. Xie, Trap Depth Engineering of SrSi2O2N2:Ln(2+),Ln(3+) (Ln(2+) = Yb, Eu; Ln(3+) = Dy, Ho, Er) Persistent Luminescence Materials for Information Storage Applications, *ACS Appl Mater Interfaces*, 2018, **10**, 1854-1864.
23. X. Zhou, L. Ning, J. Qiao, Y. Zhao, P. Xiong and Z. Xia, Interplay of defect levels and rare earth emission centers in multimode luminescent phosphors, *Nature Communications*, 2022, **13**, 7589.